An Inductive Approach to Simulating Multispectral MODIS Surface Reflectance Time Series

T.L. Grobler, *Student Member, IEEE,* E.R. Ackermann, *Student Member, IEEE,* A.J. van Zyl, J.C. Olivier, W. Kleynhans and B.P. Salmon

***Abstract*—In this paper, a first order MODIS time series simulator, which uses a Colored Simple Harmonic Oscillator, is proposed. The simulated data can be used to augment data sets so that data intensive classification and change detection algorithms can be applied without enlarging the available ground truth data sets. The simulator's validity is tested by simulating data sets of natural vegetation and human settlement areas and comparing it to the ground truth data in the Gauteng province located in South Africa. The difference found between the real and simulated data sets, which is reported in the experiments is negligent. The simulated and real world data sets are compared by using a wide selection of class and pixel metrics. In particular the average temporal Hellinger distance between the real and simulated data sets is 0.2364 and 0.2269 for the vegetation and settlement class respectively, while the average parameter Hellinger distance is 0.1835 and 0.2554 respectively.**

I. Introduction

SIMULATED data sets are used for algorithm development, testing and validation as well as for optimizing instrument specifications. Clearly simulated data is a valuable tool and can be used in the remote sensing field [1], [2].

Most remote sensing simulators use biophysical deductive models to simulate the reflectance of a specific land cover type [2], [3]. Inductive simulators can be used to complement deductive simulators. An inductive simulator does not require biophysical parameters, but rather attempts to fit an appropriate inductive mathematical model to the observed data directly. An example of such an application for an inductive simulator with respect to a deductive simulator is to simulate (forecast) a time-series of Leaf Area Index (LAI) [4], which in turn is used by a deductive simulator like PROSAIL [3].

In most cases the inductive models are used as a noise reduction tool to extract phenological markers from remotely sensed time series [5]. The Simple Harmonic Oscillator (SHO) model is an example of an inductive model [6], given by

$$A\sin(2\pi f_s t + \phi) + C. \tag{1}$$

T.L. Grobler is with the Department of Electrical, Electronic and Computer Engineering, University of Pretoria, Pretoria 0002, South Africa and also with Defence, Peace, Safety and Security, Council for Scientific and Industrial Research, Pretoria 0001, e-mail: trienkog@gmail.com.

E.R. Ackermann is with the Computational and Applied Mathematics Department at Rice University, Houston, Texas, TX 77005-1827, USA

A.J. van Zyl is with the Department of Mathematics and Applied Mathematics, University of Pretoria, Pretoria, South Africa.

J.C. Olivier is with the School of Engineering, University of Tasmania, 7001, Hobart, Australia.

W. Kleynhans and B.P. Salmon are with the Remote Sensing Research Unit, Meraka Institute, Council for Scientific and Industrial Research, Pretoria 0001, South Africa and also with the Department of Electrical, Electronic and Computer Engineering, University of Pretoria, Pretoria 0002, South Africa

Manuscript received ???, 2011.

Many other models have been proposed as an improvement to the SHO model [4], [5], [7]–[10]. In particular, Carrão *et al.* [5] modeled Moderate Resolution Imaging Spectroradiometer (MODIS) time series with a harmonic non-linear solution of a chaotic attractor. Kleynhans *et al.* [9] modeled Normalized Difference Vegetation Index (NDVI) time series with a triply modulated cosine function. Jönsson *et al.* [7] modeled vegetation index time series using asymmetric Gaussian functions, while Zhang *et al.* [8] used piecewise-defined local double logistic functions.

The objective of this paper is to use a parsimonious inductive model to *simulate multispectral time series with an inherent correlation structure*. By extending the CSHO proposed by Grobler *et al.* [10], a simulator that can *augment data sets for data intensive classification and change detection algorithms* is developed [11], [12]. The paper presents its findings by simulating time-series in the Gauteng province located in South Africa. In selective cases, statistical inductive models similar to the CSHO have been used to forecast a single time series [4]. The complex issue of incorporating multispectral correlation into a simulator was not addressed in [4]. Generating multispectral time series using the CSHO model required the addressing of a few complex issues. The proposed simulator incorporates the average class noise correlation between the different spectral bands and reproduces class specific spectral behavior by enforcing the statistical restrictions imposed by the different model parameters of each spectral band on each other. The SHO was selected as the noise free model, since the model proved sufficient in replicating the statistical characteristics of the data sets and as such it was deemed unnecessary to use the more complex non-linear models for multi-year fitting. The improvement in accuracy using a non-linear model is small and costly for a multi-year time series containing inter-annual variation with a strong sinusoidal component.

To accomplish efficient time series analysis and simulator validation, a long reliable high temporal remote sensing time series was needed and the MCD43A4 MODIS product was identified as a viable candidate and consists of Bidirectional Reflectance Distribution Function (BRDF) corrected land surface reflectance (8 day composite, 500m resolution) time series. MODIS data, when compared to Advanced Very High Resolution Radiometer (AVHRR) data, exhibits enhanced spectral and radiometric resolution, wide geographical coverage and improved atmospheric corrections, while preserving the same temporal resolution [13].

II. Data Description

The ground truth time series data is extracted from the 8-day composite MODIS MCD43A4 BRDF corrected 500 m land surface reflectance product corresponding to a total area of approximately 230 km^2 of the Gauteng province located in South Africa.[1] The temporal acquisition rate of MODIS MCD43A4 roughly translates to 45 observations per year. The most prevailing form of land cover change in South Africa is settlement expansion. Two classes of land cover type are considered: *natural vegetation* and *settlements*, denoted by v and s. The focus of this paper will be on simulating settlement and vegetation pixels, since settlement expansion is a relevant problem in South Africa. The ground truth dataset denoted by R, consists of 925 MODIS pixels and was picked by means of (human) visual interpretation of two high resolution Système Probatoire d'Observation de la Terre (SPOT) images from the year 2000 and 2008 respectively. We selected MODIS pixels that, according to the SPOT images, did not change and had the appropriate percentage land cover type in a MODIS pixel at SPOT resolution. In this study the settlements class contains pixels consisting of about 50% buildings, and 50% vegetation, whereas the vegetation class contains pixels with more than 90% vegetation. Each MODIS pixel contains eight time series (seven MODIS land bands, and Normalized Difference Vegetation Index) with $I = 368$ observations (extracted between 2000 and 2008). The NDVI time series was computed using the first two spectral land bands. The dataset R is divided into the two classes: settlements (333 pixels) and natural vegetation (592 pixels).

III. Simulator

A. Colored Simple Harmonic Oscillator

Let $\mathbf{x}_c(t) = \{x_c^b(t)\}_{b\in\{1\cdots7\}}$ denote a MODIS pixel at time t with assigned class label $c \in \mathcal{C}$, where $x_c^b(t)$ denotes the b^{th} spectral band's reflectance at time t. The c is omitted if the class of the MODIS pixel is unknown. Each observed signal belonging to the same class is a sample path of a stochastic process $X_c^b(t)$. Each MODIS class c is therefore modeled as a set of stochastic processes $\mathbf{X}_c(t) = \{X_c^b(t)\}_{b\in\{1\cdots7\}}$. Since $X_c^b(t)$ is a stochastic process we can assign an analytic expression (if such an expression exists) to each sample path (MODIS pixel) $x_c^b(t;\boldsymbol{\theta}_c^b)$ of $X_c^b(t)$, where $\boldsymbol{\theta}_c^b$ is a set of random values with a joint probability density function.

The proposed analytic expression for each MODIS pixel in each band (sample path) is given by

$$x_c^b(t;\boldsymbol{\theta}_c^b) = s_c^b(t;\{A_c^b,\phi_c^b,C_c^b\}) + \eta_c^b(t;\{\mu_c^b,\lambda_c^b,\sigma_c^b\}), \quad (2)$$

where $s_c^b(t;\{A_c^b,\phi_c^b,C_c^b\})$ is the SHO model given in (1) with period $T_s = \frac{1}{f_s} = 45$.

The noise process $\eta_c^b(t;\{\mu_c^b,\lambda_c^b,\sigma_c^b\})$ is an Ornstein-Uhlenbeck process that satisfies the stochastic differential equation

$$d\eta_c^b(t) = \lambda_c^b(\mu_c^b - \eta_c^b(t))dt + \sigma_c^b dW(t). \quad (3)$$

[1]The MODIS MCD43A4 product can be downloaded from http://modis.gsfc.nasa.gov/data/.

Here $\mu_c^b \in \mathbb{R}$ is the long-term mean of the process, $\lambda_c^b > 0$ is the rate of mean reversion, $\sigma_c^b > 0$ is the volatility or average magnitude, per square-root time, of the random fluctuations, and $W(t)$ is a standard Brownian motion on $t \in [0,\infty)$, implying that $dW(t) \sim \mathcal{N}(0,\sqrt{dt})$.

One should, for each class and band, expect μ_c^b to be insignificant relative to C_c^b, as $\mu_c^b = 0$ if the parameter C_c^b is estimated without error. For convenience $\boldsymbol{\theta}_c^b$ will sometimes be omitted from $x_c^b(t;\boldsymbol{\theta}_c^b)$.

The distribution of $\boldsymbol{\theta}_c^b$ is determined by the parameter set $\{A_c^b,\phi_c^b,C_c^b,\lambda_c^b,\sigma_c^b\}$ and it follows that $\boldsymbol{\theta}_c = \{\boldsymbol{\theta}_c^b\}_{b\in\{1\cdots7\}} = \{A_c^b,\phi_c^b,C_c^b,\lambda_c^b,\sigma_c^b\}_{b\in\{1\cdots7\}} = \{\theta_1,\cdots,\theta_{35}\}$ with a probability density function denoted by $f_c(\boldsymbol{\theta}_c)$. When NDVI is included in the parameter set the notation $\tilde{\boldsymbol{\theta}}_c$ will be used. The same convention applies for $\tilde{\mathbf{X}}_c(t)$ and $\tilde{\mathbf{x}}_c(t)$. NDVI is excluded when constructing the probability density function $f_c(\boldsymbol{\theta}_c)$, since NDVI must be constructed from band 1 and 2. NDVI is included in the similarity metrics as the real and simulated data sets must be compared as a whole. NDVI is always constructed from band 1 and 2 and is never simulated directly.

The ensemble mean for $\tilde{\mathbf{X}}_c(t)$ is defined as

$$\mathbf{y}_c(t) = \{\mathbb{E}\ [X_c^b(t)]\}_{b\in\{1\cdots7,\text{NDVI}\}} \quad (4)$$

and the autocorrelation of $\tilde{\mathbf{x}}_c(t)$ is defined as $\tilde{\mathbf{R}}_c(\tau) = \{\mathcal{R}_c^b(\tau)\}_{b\in\{1\cdots7,\text{NDVI}\}}$, where

$$\mathcal{R}_c^b(\tau) = \frac{(x_c^b(t) - \mathbb{E}[x_c^b(t)])(x_c^b(t+\tau) - \mathbb{E}[x_c^b(t)])}{\text{var}(x_c^b(t))}. \quad (5)$$

The estimation procedure of the parameters of $\mathbf{x}_c(t)$ are discussed in detail in [10]. The estimated parameters are denoted by $\hat{\boldsymbol{\theta}}_c$.

B. Parameter Probability Density Function

All the estimated parameters (of all pixels in a specific class) are represented with the vector $\boldsymbol{\Theta}_c = \{\Theta_1,\Theta_2,\cdots,\Theta_{35}\}$, where Θ_i is a random variable and θ_i is a realization of it. The joint density of $\boldsymbol{\Theta}_c$ is assumed to be Gaussian distributed and expressed with

$$f_c(\boldsymbol{\theta}_c) = \frac{1}{\sqrt{(2\pi)^{|\boldsymbol{\theta}_c|}|\boldsymbol{\Sigma}|}} \exp\left[-\frac{1}{2}(\boldsymbol{\theta}_c - \boldsymbol{\mu})\boldsymbol{\Sigma}^{-1}(\boldsymbol{\theta}_c - \boldsymbol{\mu})\right]. \quad (6)$$

In equation (6), $\boldsymbol{\mu} = \mathbb{E}[\boldsymbol{\Theta}_c]$ and $\boldsymbol{\Sigma}$ is the covariance matrix with elements $\Sigma_{n,m} = \mathbb{E}[(\Theta_n - \mu_{\Theta_n})(\Theta_m - \mu_{\Theta_m})],\ \forall m,n \in \{1,\cdots,|\boldsymbol{\theta}_c|\}$.

C. Parameter and Noise correlation

The parameter correlation matrix $\boldsymbol{P}_p^c$ has elements $P_{n,m} = \frac{\mathbb{E}[(\Theta_n - \mu_{\Theta_n})(\Theta_m - \mu_{\Theta_m})]}{\sigma_{\Theta_n}\sigma_{\Theta_m}},\ \forall m,n \in \{1,\cdots,|\boldsymbol{\theta}_c|\}$. The parameter correlation matrix $\boldsymbol{P}_p^c$ is used to get an indication of the dependence between the model parameters of each class and is used to model class specific spectral behavior.

In addition to $\boldsymbol{P}_p^c$, the noise correlation $\boldsymbol{P}_\eta^c$ is measured between the different MODIS bands. To determine the noise correlation, $dW^b(t)$ from (3) needs to be estimated, since $dW^b(t)$ induces the random behavior in the noise. To estimate

$dW^b(t)$, $\eta^b(t)$ is discretized with timesteps of length Δt. An exact formula that holds for $\Delta t = 1$ is [10]

$$\eta^b[i] = e^{-\lambda}\eta^b[i-1]+(1-e^{-\lambda^b})\mu^b+\sigma^b\sqrt{\frac{(1-e^{-2\lambda^b})}{2\lambda^b}}\Delta W^b[i], \tag{7}$$

where $\Delta W^b[i] \sim \mathcal{N}(0,1)$ and is equal to $\Delta W^b[i] = W^b[i] - W^b[i-1]$.

By making $\Delta W^b[i]$ the subject of (7), it can be used to estimate (or approximate) the *independent*, normally distributed innovation terms for each timestep of each MODIS band. This, in turn, allows the computation of the correlation matrix $\boldsymbol{P}_\eta^c$ of the innovation terms across the spectral bands with $P_{n,m} = \frac{\mathbb{E}[(\Omega_n-\mu_{\Omega_n})(\Omega_m-\mu_{\Omega_m})]}{\sigma_{\Omega_n}\sigma_{\Omega_m}}$, $\forall m,n \in \{1,\cdots,7\}$, where Ω_n is the random variable with realizations ΔW^n and n refers to the MODIS band.

D. Generating correlated innovations

The independent, correlated innovations are generated by following the approach presented in [14]. Let us therefore consider d independent standard (i.e. unit variance) white noise processes $\overline{\Delta W}^1, \ldots, \overline{\Delta W}^d$ each of length I, where I is the amount of observations one wants to simulate. Let furthermore a (deterministic and constant) matrix

$$\boldsymbol{\delta} = \begin{bmatrix} \delta_{11} & \delta_{12} & \cdots & \delta_{1d} \\ \delta_{21} & \delta_{22} & \cdots & \delta_{2d} \\ \vdots & \vdots & \ddots & \vdots \\ \delta_{71} & \delta_{72} & \cdots & \delta_{7d} \end{bmatrix} \tag{8}$$

be given, and consider the 7-dimensional processes $\boldsymbol{\Delta W}_c$, defined by

$$\boldsymbol{\Delta W}_c = \boldsymbol{\delta}\overline{\boldsymbol{\Delta W}}, \tag{9}$$

where

$$\boldsymbol{\Delta W}_c = [\Delta W_c^1 \cdots \Delta W_c^7]^T. \tag{10}$$

Let us now assume that the rows of $\boldsymbol{\delta}$ have unit length, i.e.

$$\|\delta_{i\#}\|_2 = 1, \quad i = 1,\ldots,7. \tag{11}$$

Then each of the components $\Delta W_c^1, \cdots, \Delta W_c^7$ separately are also standard (i.e. unit variance) white noise processes, with instantaneous correlation given by

$$\boldsymbol{P}_\eta^c = \boldsymbol{\delta}\boldsymbol{\delta}^*. \tag{12}$$

Given a positive definite correlation matrix $\boldsymbol{P}_\eta^c$ we can obtain $\boldsymbol{\delta}$ by using Cholesky factorization, such that (11) is automatically satisfied.

E. Simulation and Validation

The simulator is validated by using class and pixel metrics. The class metrics are used to determine whether the simulated data set have the same statistical attributes as the original data set and are important, since class attributes are used by classifiers to distinguish between classes [10], [15]. The pixel metrics in contrast are used to verify that the simulator can also reproduce any given pixel accurately by comparing every real world pixel to its simulated counterpart. The construction procedures of the simulated data sets on which the two types of metrics are applied differs and are illustrated in Figure 1.

The steps required to generate the data set S on which the class metrics is applied are summarized below:

i. Estimate the parameters of R_c (all the pixels in R belonging to class c) [10].
ii. Select a random 50% of the estimated parameters to construct $\boldsymbol{P}_p^c$. The pixels associated with the selected parameters form the training set. The remaining pixels in R_c belong to the validation set.
iii. Create $f_c(\boldsymbol{\theta}_c)$ from $\boldsymbol{P}_p^c$ (actually the parameter covariance matrix is used) using (6) and draw $N \times \boldsymbol{\theta}_c$ from it.
iv. Calculate $\mathbf{s}(t)$ with (1), by using the harmonic parameters of step i.
v. Determine the residual by subtracting $\mathbf{s}(t)$ from $\mathbf{x}(t)$.
vi. Compute $\boldsymbol{P}_\eta^c$ from the residual, by using the same training set as in step ii and (7).
vii. Calculate N time series of correlated increments $\boldsymbol{\Delta W}_c$ using $\boldsymbol{P}_\eta^c$, (9) and (12).
viii. Generate correlated noise by using the noise parameters of $\boldsymbol{\theta}_c$ (drawn in step iii), $\boldsymbol{\Delta W}_c[i]$ and (7).
ix. Create the simulated harmonic component by using the harmonic parameters of $\boldsymbol{\theta}_c$ and (1).
x. Add the correlated noise to the harmonic component.
xi. Generate NDVI from the simulated data by using band 1 and 2.

The pixel metrics simulated data set S is constructed by using a different approach. The symbol S is used in both scenarios as to avoid further clutter in the next sections. The steps required to generate the data set S on which the pixel metrics are applied are summarized below:

I-III. Follow steps i, iv and v of the class generation algorithm.
IV. Execute step vi of the class generation algorithm, but use all of the pixels in R_c.
V. Perform step vii of the class generation algorithm, but generate $|R_c|$ time series instead of N.
VI. Generate correlated noise by using the estimated noise parameters derived in step i instead of the noise parameters of $\boldsymbol{\theta}_c$.
VII. Add the correlated noise to the harmonic signal generated in step ii.
VIII. Generate NDVI from the simulated data by using band 1 and 2.

IV. Results and Discussion

Random split cross validation was performed to create 50 different class metric simulated data sets, with $N = 1000$. There was no cross validation used for the pixel metrics, since all the pixels in R_c were used. For the pixel metrics 50 independent experiments were also conducted. The class and pixel metrics were then applied on each experiment to produce the results in Table I.

A. Discussion on Metric Selection

The metrics in this section are based on the metrics proposed in [16]. Two underlying metrics are used, namely sum of

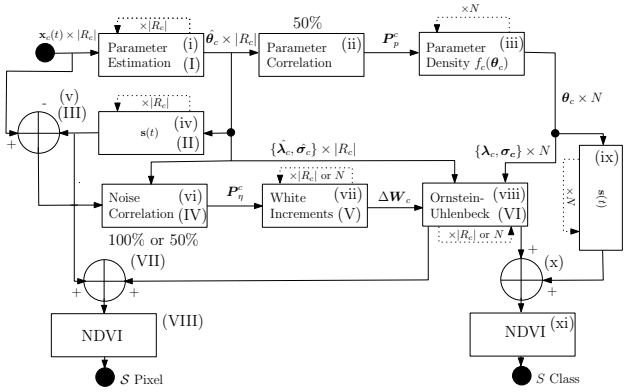

Fig. 1: Flow diagram illustrating how S is generated. When there are two possibilities at a block, the first option relates to the generation of the pixel set S, while the second option is used to create the class set S. The capital roman numerals are the steps needed to create the pixel set S, while the small letter roman numerals are the steps required to create the class set S. Furthermore $\mathbf{s}(t) = \{s^b(t)\}_{b\in\{1\cdots7\}}$, $\boldsymbol{\sigma}_c = \{\sigma_c^b\}_{b\in\{1\cdots7\}}$ and $\boldsymbol{\lambda}_c = \{\lambda_c^b\}_{b\in\{1\cdots7\}}$, while $\hat{\boldsymbol{\lambda}}_c$ and $\hat{\boldsymbol{\sigma}}_c$ are defined similarly.

squared error (SSE) and Hellinger distance (except for the power spectral density metric that measures power). In both cases a value *close to zero indicates good similarity*. When "Hellinger" is not part of the metric name it indicates that the SSE was used as the base metric. As the results in Table I are close to zero, the *results validate our simulator* for the current data sets. Each metric was chosen to verify that the simulator reproduces three important characteristics, namely temporal dynamics, spectral behavior and accurate noise.

1) Temporal Dynamics: There are two types of temporal dynamics to account for, namely intra and inter annual variation. The main reason for intra annual variation is due to seasonality, which is caused by a wide range of factors including plant phenology. The underlying noise free SHO tries to model the average seasonal behavior and has a period of one year. Inter annual variation can be caused by many factors including drought and floods. Since the CSHO is a cyclo-stationary stochastic process it can not model inter annual variation precisely, but it can represent the average behavior of multiple years by reducing the remaining harmonic information in the residual to two average parameters, namely λ_c^b and σ_c^b. If the time-series being modeled does not contain major trends, then the CSHO is an accurate first order approximation of the time-series. The *yearly ensemble mean* metric is a first order statistic and is used to verify that the average seasonal behavior is replicated correctly. The *average temporal Hellinger distance* is probably the most important metric from the perspective of [11], [12] as it measures the difference between the first order statistical description of the CSHO and the true data set. The *autocorrelation* metric is a second order statistic which measures whether the CSHO also models the temporal behavior of any given pixel properly.

2) Spectral Behavior: The paper presents an approach for simulating the spectral behavior of a specific class. We know that each class will have a unique spectral signature within a certain allowable margin of variation. The proposed simulator encapsulates and models the spectral signature for each class by using (6). Equation (6) enforces the class specific statistical restrictions imposed by the different model parameters of each spectral band on each other. The *parameter correlation metric* measures how effective the simulator is in reproducing spectral dependence, while the *average parameter Hellinger distance* measures how trustworthy the joint Gaussian assumption of $f_c(\tilde{\boldsymbol{\theta}}_c)$ is.

Furthermore the model also enforces noise correlation by using the approach presented in Sections III-C and III-D. The noise correlation metric measures how duly the noise correlation is modeled. In Fig. 2 the noise and parameter correlation matrices for the vegetation class are shown.

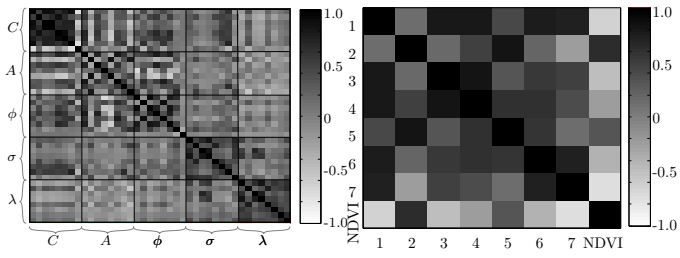

(a) Parameter correlation matrix for the vegetation class.

(b) Noise correlation matrix for the vegetation class.

Fig. 2: Parameter and noise correlation matrices for the vegetation class

3) Accurate Noise: A widely used assumption for remotely sensed time series noise is that it is white [5], [9] if all information carrying frequency components have been extracted [4]. The different *power spectral density* metric values reveal whether a white or colored assumption is more appropriate when using an SHO as underlying noise model. Table I indicate that a colored noise model is more appropriate than assuming white noise. This is as expected, since only the mean and seasonal harmonic components were extracted via the SHO. The *average noise increment Hellinger distance* determines whether the noise increments of each pixel are similar to the increments of the Ornstein-Uhlenbeck process.

B. Class Metrics

1) Yearly Ensemble Mean:
The equation for the yearly ensemble mean can be found in Table I where $\tilde{\bar{\mathbf{y}}}_c(t)$ is the yearly ensemble mean of c and is estimated by taking the average at each temporal step of MCD43A4 over all pixels and then over all years (see Table I). To determine the sum of squared error (SSE) of each time step in the year we need to divide the metric in Table I by 45. The settlement class has a slightly higher variance due to the fewer samples that are available for the settlement class.

2) Average Parameter Hellinger Distance:
The equation for the average parameter Hellinger distance can be found in Table I, where $f_c(\theta_k)$ is the marginal probability density function of $f_c(\tilde{\boldsymbol{\theta}}_c)$ and $\mathrm{HD}(f_c^{R_c}(\theta_k), f_c^S(\theta_k))$ represents the Hellinger distance between $f_c^{R_c}(\theta_k)$ and $f_c^S(\theta_i)$.

3) Noise and Parameter Correlation metrics: The equations for the noise and Parameter Correlation metrics are given in Table I. The noise correlation metric needs to be divided by 8×8 (NDVI was added for completeness), while the parameter correlation metric needs to be divided by 40×40 to determine the average SSE.

4) Average Temporal Hellinger distance: The equation for the average temporal Hellinger distance can be found in Table I, where $f_{x_c^b(t)}$ is the probability density function in band b at time step t, with $b \in \{1,\cdots,7,\text{NDVI}\}$.

C. Pixel Metrics

1) Autocorrelation: The equation for autocorrelation metric can be found in Table I. To determine the average SSE per lag value we need to divide the autocorrelation metric by 368 (amount of observations).

2) Average Noise increment Hellinger distance: The equation for the average noise increment Hellinger distance can be found in Table I, where $f_{\Delta\eta^b}^{R_c(p)}$ is the density function of the noise increments $\eta^b[t+1]-\eta^b[t]$ for pixel p in data set R_c, with $b \in \{1,\cdots,7,\text{NDVI}\}$.

3) Power Spectral Density:
The equation for the power can be found in Table I, where $D_b^{R_c^\eta(p)}(f)$ is the power spectral density of the estimated noise of pixel p in data set R_c in band b, with $b \in \{1,\cdots,7,\text{NDVI}\}$. The same metric can be applied on S^η and W^η, where W^η is the white noise model of R_c^η.

TABLE I: Difference metrics between R and S (50 experiments). The v index stands for vegetation, while the s index stands for settlement. There is no standard deviation for the Power in R_c^η as the entire set was used (and no artificial noise was added).

Metric / Equation	$\frac{\mathbb{E}[\text{Metric}]}{\sigma_{\text{Metric}}}$	
	v	s
Ensemble Mean $\int_0^I \lVert\bar{\tilde{\boldsymbol{y}}}_c^{R_c}(t)-\bar{\tilde{\boldsymbol{y}}}_c^{S}(t)\rVert_2^2 dt$	56.7015 9.5969	59.0293 31.6211
Parameter Hellinger Distance $\frac{1}{\lvert\tilde{\boldsymbol{\theta}}_c\rvert}\sum_{k=1}^{\lvert\tilde{\boldsymbol{\theta}}_c\rvert}\text{HD}(f_c^{R_c}(\theta_k),f_c^{S}(\theta_k))$	0.1835 0.0065	0.2554 0.0087
Parameter Correlation $\lVert\tilde{\boldsymbol{P}}_{p_{R_c}}^c-\tilde{\boldsymbol{P}}_{p_S}^c\rVert_2^2$	18.3972 2.4220	32.0627 5.3703
Noise Correlation $\lVert\tilde{\boldsymbol{P}}_{\eta_{R_c}}^c-\tilde{\boldsymbol{P}}_{\eta_S}^c\rVert_2^2$	0.0354 0.0074	0.0666 0.0136
Temporal Hellinger Distance $\frac{1}{8}\sum_{b=1}^{8}\frac{1}{I}\int_0^I \text{HD}(f_{x_c^b(t)}^{R_c},f_{x_c^b(t)}^{S})\ dt$	0.2364 0.0030	0.2269 0.0111
Autocorrelation $\frac{1}{\lvert R_c\rvert}\sum_{p=1}^{\lvert R_c\rvert}\int_0^I \lVert\tilde{\mathbf{R}}_c^{R_c(p)}(\tau)-\tilde{\mathbf{R}}_c^{S(p)}(\tau)\rVert_2^2\ d\tau$	31.0636 0.3421	34.3365 0.4536
Noise Hellinger Distance $\frac{1}{8}\sum_{b=1}^{8}\frac{1}{\lvert R_c\rvert}\sum_{p=1}^{\lvert R_c\rvert}\text{HD}(f_{\Delta\eta^b}^{R_c(p)},f_{\Delta\eta^b}^{S(p)})$	0.1675 0.0003	0.1755 0.0003
Power in R_c^η $\frac{1}{8}\sum_{b=1}^{8}\frac{1}{\lvert R_c\rvert}\sum_{p=1}^{\lvert R_c\rvert}\int_0^{0.1} D_b^{R_c^\eta(p)}(f)\ df$	92.7649 –	38.3202 –
Power in S^η	94.6893 0.5608	45.9516 0.2873
Power in W^η	22.9837 0.0797	11.7950 0.0472

V. Conclusion

The paper presented a simulator able to artificially generate MODIS MCD43A4 time series, and explained the need and justification for its development. The model presented in [10] was used as the core of the simulator. To test the validity of the simulator a test case was employed, where vegetation and settlement data were simulated for the Gauteng province located in South Africa. The simulated data was then compared to the real world data set R. It was shown using different simulated data sets that the differences between the real and simulated data sets are small and stable validating the simulator for the test case used in this paper.

References

[1] J. Schott, S. Brown, R. Raqueño, H. Gross, and G. Robinson, "An advanced synthetic image generation model and its application to multi/hyperspectral algorithm development," *Canadian Journal of Remote Sensing*, vol. 15, pp. 99–101, 1999.

[2] L. Guanter, K. Segl, and H. Kaufmann, "Simulation of Optical Remote-Sensing Scenes With Application to the EnMAP Hyperspectral Mission," *IEEE Transactions on Geoscience and Remote Sensing*, vol. 47, no. 7, pp. 2340–2351, 2009.

[3] W. Verhoef and H. Bach, "Coupled soil-leaf-canopy and atmosphere radiative transfer modeling to simulate hyperspectral multi-angular surface reflectance and TOA radiance data," *Remote Sensing of Environment*, vol. 109, pp. 166–182, 2007.

[4] B. Jiang, S. Liang, J. Wang, and Z. Xiao, "Modeling MODIS LAI time series using three statistical methods," *Remote Sensing of Environment*, vol. 114, pp. 1432–1444, 2010.

[5] H. Carrão, P. Gonçalves, and M. Caetano, "A Nonlinear Harmonic Model for Fitting Satellite Image Time Series: Analysis and Prediction of Land Cover Dynamics," *IEEE Transactions on Geoscience and Remote Sensing*, vol. 48, no. 4, pp. 1919–1930, Apr. 2010.

[6] J. F. Hermance, R. W. Jacob, B. A. Bradley, and J. F. Mustard, "Extracting Phenological Signals From Multiyear AVHRR NDVI Time Series: Framework for Applying High-Order Annual Splines With Roughness Damping," *IEEE Transactions on Geoscience and Remote Sensing*, vol. 45, no. 10, pp. 3264–3276, Oct. 2007.

[7] P. Jönsson and L. Eklundh, "Seasonality Extraction by Function Fitting to Time-Series of Satellite Sensor Data," *IEEE Transactions on Geoscience and Remote Sensing*, vol. 40, no. 8, pp. 1824–1832, Aug. 2002.

[8] X. Zhang, M. A. Friedl, C. B. Schaaf, A. H. Strahler, J. C. F. Hodges, F. Gao, B. C. Reed, and A. Huete, "Monitoring vegetation phenology using MODIS," *Remote Sensing of Environment*, vol. 84, no. 3, pp. 471–475, Mar. 2003.

[9] W. Kleynhans, J. C. Olivier, K. J. Wessels, F. van Den Bergh, B. P. Salmon, and K. C. Steenkamp, "Improving Land Cover Class Separation Using an Extended Kalman Filter on MODIS NDVI Time-Series Data," *IEEE Geoscience and Remote Sensing Letters*, vol. 7, no. 2, pp. 381–385, Apr. 2010.

[10] T. L. Grobler, E. R. Ackermann, A. J. van Zyl, J. C. Olivier, and W. Kleynhans, "Land Cover Separability Analysis of MODIS Time Series Data using a combined Simple Harmonic Ossilator and a mean reverting stochastic process," *IEEE Journal of Selected Topics in Applied Earth Observations And Remote Sensing*, vol. 5, no. 3, pp. 857–866, 2012.

[11] E. R. Ackermann, "Sequential land cover classification," Master's thesis, University of Pretoria, 2011.

[12] T. Grobler, E. R. Ackermann, A. van Zyl, J. C. Olivier, W. Kleynhans, and B. P. Salmon, "Using Page's Cumulative Sum Test and MODIS time series to detect land cover changes," *Geoscience and Remote Sensing Letters*, in press, DOI: 10.1109/LGRS.2012.2205556.

[13] H. Carrão, P. Gonçalves, and M. Caetano, "Contribution of multispectral and multitemporal information from MODIS images to land cover classification," *Remote Sensing of Environment*, vol. 112, pp. 986–997, 2008.

[14] T. Björk, *Arbitrage theory in continuous time*. Oxford University Press, USA, 2009.

[15] E. R. Ackermann, T. Grobler, A. J. van Zyl, J. C. Olivier, and K. C. Steenkamp, "Minimum error land cover separability analysis and classification of MODIS time series data," in *Proceedings of IEEE Geoscience and Remote Sensing Symposium*, Vancouver, Canada, July 2011, pp. 2999–3002.

[16] S. Lhermitte, J. Verbesselt, W. Verstraeten, and P. Coppin, "A comparison of time series similarity measures for classification and change detection of ecosystem dynamics," *Remote Sensing of Environment*, vol. 115, pp. 3129–3152, 2011.